Energy 238 (2022) 121716

Contents lists available at ScienceDirect

Energy

journal homepage: www.elsevier.com/locate/energy

Multi-objective robust optimization of a solar power tower plant under uncertainty

Yan Luo [a], Zhiyuan Wang [a], Jiamin Zhu [a], Tao Lu [a], Gang Xiao [b], Fengming Chu [a, **], Ruixing Wang [c, d, *]

[a] School of Mechanical and Electrical Engineering, Beijing University of Chemical Technology, Beijing, 100029, China
[b] State Key Laboratory of Clean Energy Utilization, Zhejiang University, Hangzhou, 310027, China
[c] Key Laboratory for Mechanics in Fluid-Solid Coupling Systems, Institute of Mechanics, Chinese Academy of Sciences, Beijing, 100190, China
[d] School of Engineering Sciences, University of Chinese Academy of Sciences, Beijing, 100049, China

ARTICLE INFO

Article history:
Received 21 February 2021
Received in revised form
16 July 2021
Accepted 5 August 2021
Available online 10 August 2021

Keywords:
Solar power tower plant system
Uncertainty propagation
Multi-objective robust optimization
Global sensitivity analysis
Levelized cost of energy

ABSTRACT

The optimal design of a molten salt solar power tower (SPT) plant is sensitive to the variations of uncertainties, such as solar radiation, which result in dispersion of the model output. To mitigate the impacts of uncertainties on the thermo-economic performance of SPT plant, this study develops an uncertainty-based multi-objective robust optimization design method for the case of a SPT plant in Sevilla with the expected value (i.e. the average energy cost) and the standard deviation (i.e. the dispersion of the model output) of the levelized cost of energy (*LCOE*) as the objectives. The Monte Carlo (MC) simulation and simulated annealing (SA) algorithm are combined to solve the robust optimization problem. The results of Pareto frontier indicate that a trade-off is needed through decision-making. The final optimal solution is determined with expectation of *LCOE* of 23.09 c/kWh$_e$ and standard deviation of *LCOE* of 1.25 c/kWh$_e$. Compared with the deterministic optimal design, the standard deviation of *LCOE* of the multi-objective robust optimum is reduced by 17.22 %, which turns out to be less sensitive to the uncertainties. Moreover, the Sobol' global sensitivity analysis results show that the direct solar radiation, heliostat field cost and receiver cost are the most sensitive to *LCOE*.

1. Introduction

Concentrating solar power (CSP) with thermal storage is increasingly being considered an effective method for the future development of the electricity market [1]. The International Energy Agency estimates that CSP with storage will have a global electricity market share of up to 11 % by 2050 [2]. Among different CSP applications, solar power tower (SPT) technology is growing faster than any other technology because of its higher overall efficiency and higher operating temperature [3]. The SPT plant system applies heliostats to concentrate solar energy onto a receiver in the tower, where a liquid is heated. Then the heat transfer liquid is used to generate steam, which drives turbines to generate electricity.

In recent years, many efforts have been made on the optimization of the SPT plant system [4–9]. Spelling et al. [4] described a multi-objective thermo-economic optimization scheme to determine the Pareto-optimal solution of a combined-cycle SPT plant design by employing a global evolutionary algorithm. Ramos and Ramos [5] applied local and global optimization algorithms to minimize the levelized cost of electricity (*LCOE*) of an entire SPT plant. Luo et al. [6] proposed a combined global sensitivity analysis and optimization strategy to gain the minimum *LCOE* of a SPT system. Considering exergy efficiency of the whole SPT system as objective function, Wang and He [7] conducted the optimization process of an integrated SPT system by genetic algorithm. Carrizosa et al. [8] alternatively optimized the receivers and the heliostat field by a greedy-based heuristic method with the *LCOE* as objective parameter. Through a combination of genetic and teaching-learning-based optimization algorithms, Khosravi et al. [9] gained the optimum design parameters of a SPT plant to reach the minimum *LCOE*.

* Corresponding author. Key Laboratory for Mechanics in Fluid-Solid Coupling Systems, Institute of Mechanics, Chinese Academy of Sciences, Beijing, 100190, China.
** Corresponding author. School of Mechanical and Electrical Engineering, Beijing University of Chemical Technology, Beijing, 100029, China.
E-mail addresses: cfm@mail.buct.edu.cn (F. Chu), wangruixing@imech.ac.cn (R. Wang).

https://doi.org/10.1016/j.energy.2021.121716
0360-5442/

Nomenclature

Abbreviations

CSP	Concentrating solar power
LCOE	Levelized cost of energy
MC	Monte Carlo
OLH	Optimal Latin hypercube
SA	Simulated annealing
SPT	Solar power tower

Symbols

A	area, m^2
D	standard deviation of energy cost, c/kWh_e
DNI	direct normal irradiance, W/m^2
E	expected value of energy cost, c/kWh_e
H	equivalent hours of thermal energy storage, h
h	mixed convection heat transfer coefficient, W/m^2 K
l	heliostat diagonal, m
M	number of basis functions
N	maximum number of runs of a Monte Carlo simulation
n_{hel}	total number of heliostats
p	deterministic system parameter
$\tilde{p}$	system parameter that incorporates uncertainty
Q	solar energy on the receiver surface, W
R	radius of the receiver, m
r	radius of the heliostat row, m
S	first-order sensitivity index
S_T	total sensitivity index
SM	solar multiples
T	temperature, K
THT	tower optical height, m
x	design parameter
Y	deterministic model output
$\tilde{Y}$	model output that incorporates uncertainty

Greek letters

α	receiver coating absorptance
β	regression coefficient
Δr	radial spacing between consecutive rows, m
$\Delta\gamma$	transition spacing between consecutive zones, m
$\Delta\theta$	azimuth spacing between adjacent heliostats of the same row, rad
δ	statistical error between the actual and approximate values, c/kWh_e
ε	receiver coating emittance
η	efficiency
σ	Boltzmann constant, W/m^2 K^4
ϕ	basis function

Subscripts

amb	ambient air
field	heliostat field
hel	heliostat
in	incident
rec	receiver
w	outer tube wall

Generally, in the deterministic optimization of the SPT plant system, the input system parameters are treated as constants. However, due to variation of natural conditions and development of technique economics, input parameters in real SPT plant system design are inevitably affected by uncertainties and should be assigned with probability distributions. For instance, the solar radiation obtained by ground measurements and satellite data in solar thermal design is a typical uncertain parameter with a relative root mean squared error of 5.4 % [10,11]. Another important uncertain variable is the cost of the SPT plant subsystem, such as heliostat field cost, which is generally endowed uniform probability distributions [12,13]. Besides, other input factors, such as heliostat cleanliness, receiver coating absorptance and the performance of the solar receiver, all usually deviate from their nominal values [12–15].

These uncertainties can cause dispersion of the solar thermal plant system model output, which is different from the deterministic result. The impacts of uncertainties on the model output have been investigated by some researchers [12,16–19]. Ho and Kolb [12] obtained that the actual *LCOE* of a 100MW_e SPT plant ranged from 0.11 \$/kWh_e to 0.15 \$/kWh_e under uncertain environment of annual energy and cost, while the deterministic result of *LCOE* was 0.12 \$/kWh_e. Meybodi and Beath [16] evaluated the influences of cost uncertainties and solar data variations on the economics of a 30 MW_e SPT plant in Alice Springs. They found that the maximum deviation of the actual *LCOE* could be up to 22.75 % by incorporating uncertainties when compared with the deterministic *LCOE*. Zaversky et al. [17] selected five uncertain solar field performance parameters (e.g. mirror cleanliness) as probabilistic model input parameters for a parabolic trough collector power plant. They gained that the actual annual net electric energy output under uncertainty was in between the range from 149,540 MWh to 161,028 MWh, while the deterministic design result was 155,712 MWh. Silva et al. [18] and Nojavan et al. [19] also discovered that uncertain variables could induce the large dispersion of the CSP plant model output, which was different from that of deterministic result. As a result, it leads to the necessity of coupling uncertainties in the solar thermal power plant system optimization model to better reflect actual conditions.

To handle this issue, the robust optimization design based on uncertainty should be developed to decrease the dispersion of model output [20,21]. Currently, the robust optimization method has been widely applied in various energy systems [22–28]. Wang et al. [22] proposed a combined multi-objective optimization and robustness analysis method with uncertainties of meteorological data and energy demands for a building integrated energy system. They obtained that the ranges of the objective annual carbon emissions were 1674–2575 tons/year for the deterministic optimum, while that for the robust optimum were narrowed and 1740–2419 tons/year. Akbari et al. [23] took demand side, costs and tariffs structure uncertainties into consideration in the robust optimization of a building energy system and presented that the standard deviation of objective function in robust solution and deterministic solution were 190,458 \$ and 197658.5 \$, respectively. Reich et al. [24] conducted robust optimization of the district heating networks under uncertainty and found that the robust optimum reduced the standard deviation of the heat price by about 53 % when compared with the deterministic optimum. Sy et al. [25] employed uncertainties to develop a target-oriented robust optimization model for synthesis of polygeneration plants and concluded that the standard deviation of profit for the robust solution was 14.91 % less than that for the deterministic solution.

Serafino et al. [26] pointed out that the optimal geothermal organic rankine cycle design delivered by the robust optimization strategy outperformed the one derived from the deterministic optimization approach and reduced the standard deviation of the power production by 8.5 %. Therefore, the robust optimum is less sensitive to the uncertainties when compared with the deterministic optimal design. However, no studies are found to address the uncertainties at the optimization design stage of the SPT plant system. Thus the robust optimization design based on uncertainty should be used to improve the SPT plant design.

Another issue is that the vast majority of solar thermal plant analysis quantify and rank the uncertainty contributions to the system model output dispersion by stepwise linear regression sensitivity method, which is generally suitable for linear models and may result in inaccurate sensitivity results for the complex nonlinear solar thermal power plant system [29]. Ho et al. [12–14] and Wagner et al. [30] performed sensitivity studies of uncertain parameters for a SPT plant using stepwise linear regression analysis. Zaversky et al. [17] and Eck et al. [31] also applied the stepwise linear regression to conduct sensitivity analysis of uncertainties for the parabolic trough collector power plant. Therefore, to accurately assess and evaluate the relative importance of uncertainties for the SPT plant system, a new advanced global sensitivity analysis method that is fit for nonlinear model should be developed.

The main goal of the present work is to conduct multi-objective robust optimization of the SPT plant system under uncertainty, which simultaneously minimizing the expectation and standard deviation of *LCOE*, thus reducing the sensitivity of the optimal design to uncertain parameters. For that purpose, the uncertainties are assigned probability distributions, and an uncertainty propagation analysis method is used to obtain the expected value and standard deviation of *LCOE* by combining the response surface approximation model and Monte Carlo (MC) simulation. The uncertainty propagation analysis is then coupled with the multi-objective algorithm of simulated annealing (SA), allowing to determine the optimal design. Moreover, the importance ranking of the SPT plant uncertain parameters are obtained by Sobol' global sensitivity method, through which the nonlinearity of the SPT system model and the interaction effects among uncertainties are carefully considered. The reminder of the paper is structured as follows. In section 2, a deterministic model of the SPT plant system is first demonstrated and expressed as a function of 12 design parameters. Section 3 presents different sources of uncertainty in the SPT plant system and describes the uncertainty propagation method. The multi-objective robust optimization strategy under uncertainty is described in Section 4. Finally, Section 5 gives the main results of the uncertain and deterministic optimal design, as well as the global sensitivity analysis of uncertain parameters. As shown in this paper, a lower economic risk exists in the multi-objective robust optimal design under uncertainty.

2. Deterministic model of the SPT plant system

Fig. 1 depicts a typical molten salt SPT plant system, which is composed of a heliostat field with a surrounding radial staggered layout, an external receiver, a two-tank thermal storage system and a power block with a steam extraction regenerative cycle. The plant is located in Sevilla (37.4°N, 5.9°W), a city in the south of Spain with a yearly solar irradiation value of over 1700 kWh/m^2.

The heliostat field has a fixed number of 2650 heliostats and is composed of three zones with identical radial and azimuth spacing. Based on a given azimuth spacing, radial spacing and transition spacing, the heliostat field layout is obtained, and its efficiency η_{field} is calculated by the convolution method [32]. Then the incident energy onto the receiver Q_{in} can be given as follows,

$$Q_{in} = N_{hel} A_{hel} DNI \eta_{field} \tag{1}$$

where N_{hel} is the total number of heliostats, A_{hel} is the area of a heliostat (12.84 × 9.45 m^2) and *DNI* is the direct normal irradiance.

Once the receiver radius R and outer tube wall temperature T_w is given, the thermal efficiency of the receiver η_{rec} is evaluated by Ref. [33],

$$\eta_{rec} = \alpha - \frac{\varepsilon \sigma A_{rec}\left(T_w^4 - T_{amb}^4\right) + hA_{rec}(T_w - T_{amb})}{Q_{in}} \tag{2}$$

where α is the receiver coating absorptance, ε is the receiver coating emittance, σ is the Boltzmann constant, A_{rec} is the area of the receiver, h is a mixed convection coefficient that combines natural convection and forced convection heat transfer [34], and T_{amb} is the ambient air temperature.

For the two-tank thermal storage system, the design temperatures of the hot molten salt tank and the cold molten salt tank are 565 °C and 290 °C, respectively. The thermal storage capacity is characterized by the supply hours of thermal storage energy (H). The two-tank thermal storage system is well-insulated and its efficiency is assumed to be 100 % [7]. For the power block, the turbine inlet parameters are set to 12.5 MPa and 538 °C at the design point, resulting in a gross first-law cycle efficiency of 0.4018 [35]. The rated electricity output of the power block is the ratio of the electricity produced by the heliostat field at the design condition to the solar multiples (*SM*).

Based on the above subsystem models, the annual electricity output is computed as an energy-oriented performance indicator of the SPT plant. Then, an economic analysis is conducted to assess the main model output parameter *LCOE*. The expected lifetime of the SPT system is considered to be 30 years. The total investment of the plant involves indirect and direct costs, and specific cost models were reported by Ref. [36]. The costs for plant operation and maintenance are estimated to be 1 % of the total plant capital cost [37]. The model output parameter *LCOE* is calculated as follows,

$$LCOE = \frac{\text{annual capital costs} + \text{annual O\&M costs}}{\text{annual electricity output}} \tag{3}$$

In the deterministic model, the mathematical expression of the SPT plant system is formulated as,

$$Y = f(\boldsymbol{x}, \boldsymbol{p}) \tag{4}$$

where Y is the deterministic model output *LCOE*. $\boldsymbol{x}$ is a vector of design parameters, $\boldsymbol{x} = (x_1, x_2, \cdots, x_{12})$. The value ranges of the design parameters are shown in Table 1 $\boldsymbol{p}$ is a vector of system parameters, $\boldsymbol{p} = (p_1, p_2, \cdots, p_{14})$, such as receiver coating absorptance, tower cost and heliostat cleanliness. The system parameters are given specific values in the deterministic model.

3. Uncertainty quantification of the SPT plant system

3.1. Characteristics of the uncertainties

Due to the uncertainty of the system parameters, there is a large dispersion of the model output. To conduct an uncertainty quantification of the SPT plant system, the first step is to characterize the uncertainties. For the SPT plant system, 14 uncertain system parameters are chosen and characterized with probability distributions. The central values and probability distributions of uncertainties are illustrated in Table 2.

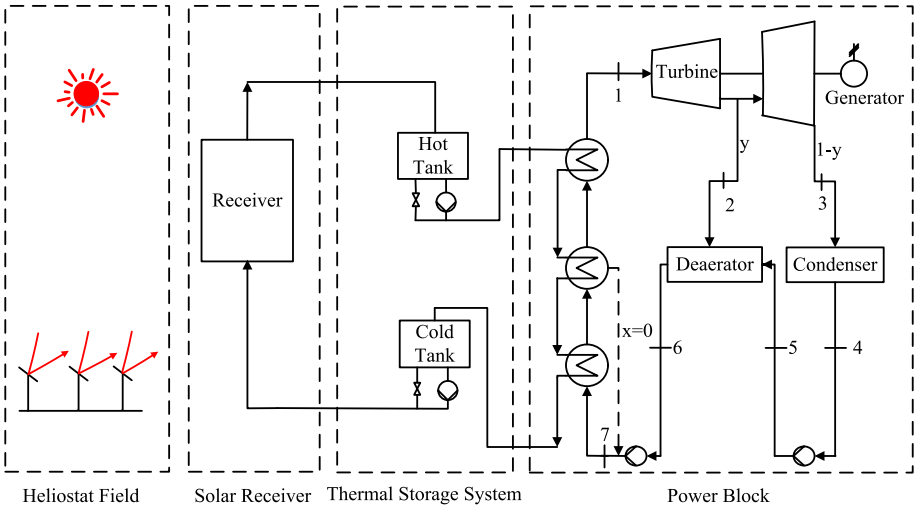

Fig. 1. Molten salt SPT plant system with thermal storage.

Table 1
Value ranges of design parameters for the SPT plant.

	Design parameter	Value range
x_1-x_3	$\Delta\theta_k$: Azimuth spacing of the k-th zone (rad) (k = 1, 2, 3)	$[l/r_k, 2l/r_k]$[a]
x_4-x_6	Δr_k: Radial spacing of the k-th zone (m) (k = 1, 2, 3)	[0.866l, 2.4l]
x_7-x_8	$\Delta\gamma_k$: Transition spacing between the k-th zone and the (k+1)th zone (m) (k = 1, 2)	[0.866l, 2.4l]
x_9	R: Receiver radius(m)	[3,5]
x_{10}	THT: Tower height (m)	[125, 165]
x_{11}	H: Supply hours of thermal storage energy (h)	[3,12]
x_{12}	SM: Solar multiples (−)	[1.3, 2.7]

[a] l represents the heliostat diagonal, and r_1 is the horizontal distance from the tower to the first row of the heliostat field.

Table 2
Probability distributions of uncertainties for the SPT plant system.

	Uncertain parameter	Central value	Distribution
$\tilde{p}_1$	Direct radiation (kWh/m^2)	Weather database [38]	Normal ±5.4 % [11]
$\tilde{p}_2$	Land cost ($/m^2)	1.25 [36]	Uniform ±15 % [12]
$\tilde{p}_3$	Heliostat improvement cost ($/m^2)	20 [36]	Uniform ±15 % [12]
$\tilde{p}_4$	Heliostat field cost ($/m^2)	200 [36]	Uniform ±18 % [12]
$\tilde{p}_5$	Receiver cost ($)	$83.34 \times \left(\frac{A_{rec}}{1133}\right)^{0.7}$ [36]	Uniform ±20 % [12]
$\tilde{p}_6$	Tower cost ($)	$0.0018357 \cdot THT^2 - 0.285868 \cdot THT + 30$ [36]	Uniform ±15 % [12]
$\tilde{p}_7$	Thermal storage cost ($/kWh$_{th}$)	30 [36]	Uniform ±14 % [12]
$\tilde{p}_8$	Power generation unit cost ($/kW$_e$)	1000 [36]	Uniform ±14 % [12]
$\tilde{p}_9$	Steam generation cost ($/kW$_e$)	350 [36]	Uniform ±23 % [12]
$\tilde{p}_{10}$	Receiver coating absorptance (−)	0.95 [36]	Uniform 0.93−0.97 [12]
$\tilde{p}_{11}$	Receiver coating emittance (−)	0.95 [33]	Uniform 0.93−0.97 [12]
$\tilde{p}_{12}$	Receiver thermal loss (MW)	Calculated by receiver performance model [33]	Uniform ±24 % [12]
$\tilde{p}_{13}$	Heliostat cleanliness (−)	0.95 [36]	Uniform 0.93−0.97 [12]
$\tilde{p}_{14}$	Heliostat optical error (mrad)	2.9 [39]	Uniform ±50 % [14]

3.2. Uncertainty propagation

Fig. 2 shows the uncertainty propagation process for the SPT plant system. The design parameters are characterized by specific values, while uncertain system parameters are defined as normal or uniform distributions. These input uncertainties induce dispersion of the model output through the SPT plant model and the probability distribution of the model output is estimated by a statistical simulation method. Among the different statistical simulation methods, the MC simulation [40] is considered the most accurate approach and selected to conduct uncertainty propagation process.

The calculation procedure of the MC simulation is shown in Fig. 3 and can be explained as follows.

1) The characteristics of the input parameters are assigned.
2) The maximum number of runs of a MC simulation N is defined and set to $m = 1$ (the value of N is generally equal to 1000 when both the accuracy and computational time are considered).
3) By applying a type of sampling technique, a random sequence is generated between 0 and 1. Sampling techniques usually include simple random sampling, descriptive sampling and Sobol sampling [41]. Sobol sampling is adopted in this paper because samples obtained using Sobol sequences are more

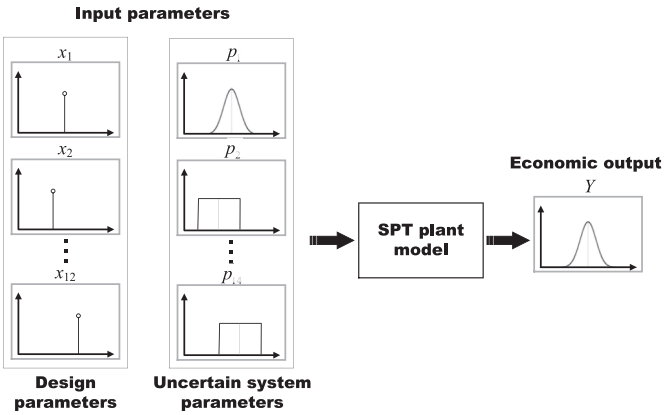

Fig. 2. Uncertainty propagation for the SPT plant system.

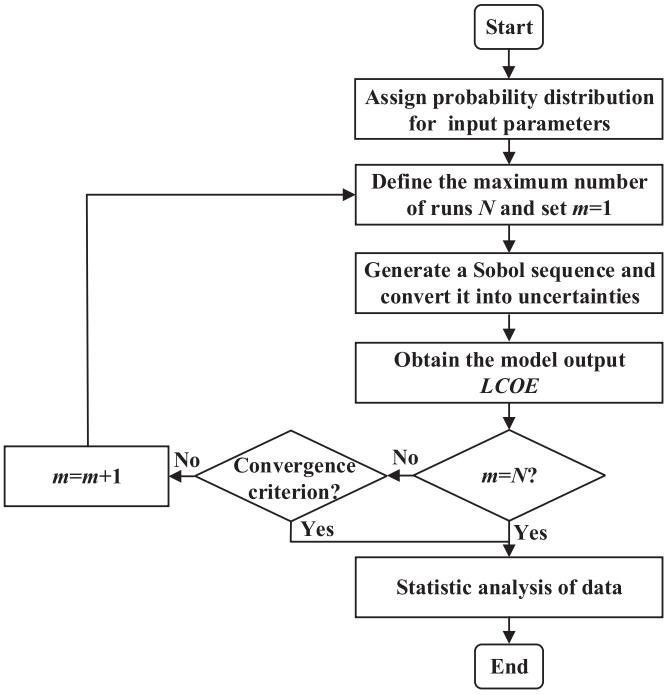

Fig. 3. Flowchart of the MC simulation.

uniformly distributed than those obtained from the other two sampling techniques.

4) The Sobol sequence is converted to the corresponding uncertain parameter values.
5) The model output *LCOE* is obtained based on a simulation of the SPT plant system model under uncertainty.
6) Let $m = m+1$ and repeat steps 3 to 5 until the maximum number of runs of a MC simulation N is reached or the solution is converged.
7) The expected value and standard deviation of the model output *LCOE* are analysed.

Once the uncertainty propagation process is conducted, the mathematical formulation of the SPT plant system under uncertainty is given by,

$$\tilde{Y} = f(\boldsymbol{x}, \tilde{\boldsymbol{p}}) \tag{5}$$

where $\tilde{Y}$ is a function that quantifies the impact of system uncertainties on the model output *LCOE* and $\tilde{\boldsymbol{p}}$ is a vector of system parameters that incorporates uncertainty.

3.3. Approximation model

To carry out the uncertainty propagation of the SPT plant system in a computationally inexpensive manner, an approximation function is used to create the surrogate model of the SPT plant system under uncertainty. Among various approximation functions, the response surface methodology [42] is applied because of its high efficiency and good robustness. The response surface methodology develops a relationship between input factors ($\boldsymbol{x}\tilde{\boldsymbol{p}}$) and the model output ($\tilde{Y}$) with a high-order polynomial function, which can be given by,

$$\tilde{Y} = \sum_{J=1}^{M} \beta_J \phi_J(\boldsymbol{x}, \tilde{\boldsymbol{p}}) + \delta \tag{6}$$

where β_J is the regression coefficient to be determined by the least squares method, $\phi_J(\boldsymbol{x}, \tilde{\boldsymbol{p}})$ is the basis function of $\boldsymbol{x}$ and $\tilde{\boldsymbol{p}}$, δ is the statistical error between the actual and approximate values of the model output *LCOE*, and M is the number of terms of $\phi_J(\boldsymbol{x}, \tilde{\boldsymbol{p}})$.

Before constructing the response surface approximation function, the sampling points of the design parameters and uncertain parameters are generated through an experimental design. Due to the advantages of uniformity of samples and low computational cost, the optimal Latin hypercube (OLH) method is chosen for experimental design [43]. A sampling input data set of 4000 points is generated to establish a quadratic polynomial response surface of the SPT plant system model under uncertainty. To validate the approximation model, 430 sampling points are generated to conduct error analysis. Fig. 4 illustrates comparison results of the approximate *LCOE* obtained by the response surface methodology and the actual *LCOE* obtained by model simulation. It can be seen that there is good agreement between the approximation and

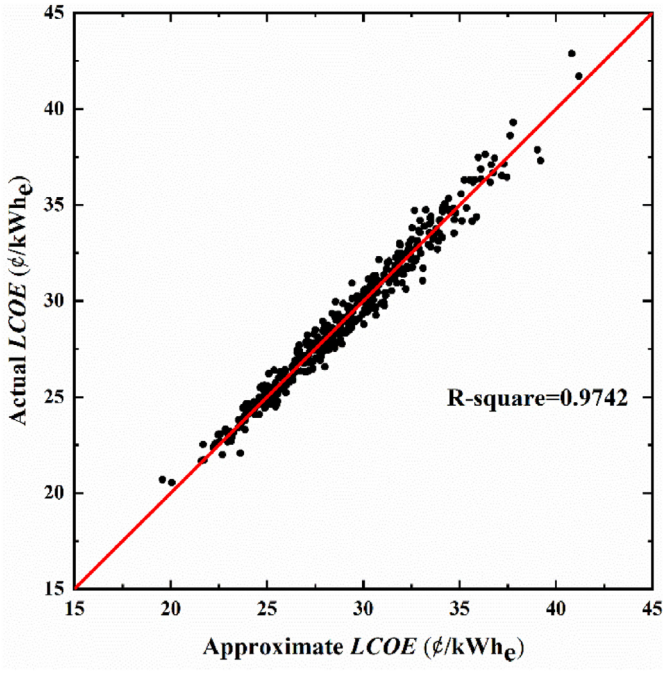

Fig. 4. Approximate and actual values of the model output *LCOE*.

simulation models, with a R-squared value of 0.9742.

4. Multi-objective robust optimization model of the SPT plant system under uncertainty

In order to design a SPT plant system with a low economic risk under uncertainty, a robust optimization design [20,21] strategy is considered. As illustrate in Fig. 5, the concept of the robust optimization design is to reduce the sensitivity of model output to uncertainties (i.e. standard deviation of model output) and optimize the performance of model output (i.e. expected value of model output), which result in a multi-objective optimization problem.

Based on the robust optimal design, the SPT plant system optimization under uncertainty is conducted by considering both the expected value and the standard deviation of *LCOE* as objective parameters, and described by,

$$\text{Minimize}: \begin{cases} E\left(\tilde{Y} = E\left(f\left(\boldsymbol{x}, \tilde{\boldsymbol{p}}\right)\right)\right) \\ D\left(\tilde{Y}\right) = D\left(f\left(\boldsymbol{x}, \tilde{\boldsymbol{p}}\right)\right) \end{cases} \quad (7)$$

$$\text{Subject to: } x_i^L \le x_i \le x_i^U,\ i = 1, 2, \ldots, 12$$

where E and D represent the expected value and standard deviation of *LCOE*, respectively. x_i^L and x_i^U are lower and upper bound of design parameter, respectively.

To solve the multi-objective robust optimization problem of the SPT plant system under uncertainty, an algorithm is required to obtain the Pareto optimal points, which are the non-inferior solutions that are searched in the whole design space. Because of high efficiency and good applicability, a SA optimization strategy is employed and the calculation procedure can be summarized as follows [44,45],

1) Select a starting point $\boldsymbol{x}^0$ and an initial temperature t_0. Initialize the optimal value $x^{\text{opt}} = x^0$, and evaluate the corresponding objective values. Let $j = 0$, and set the maximum iterative step to be L.
2) A random point $\boldsymbol{x}^*$ is generated around $\boldsymbol{x}^j$, and the corresponding objective values are obtained.
3) The random point $\boldsymbol{x}^*$ is compared with the Pareto optimal set. If $\boldsymbol{x}^*$ is a non-inferior solution, update the Pareto optimal set, and let $x^{j+1} = x^*$. If not, $\boldsymbol{x}^*$ is set to the new solution based on the Metropolis criterion [46].
4) If $j \ge L$, a new initial point $\boldsymbol{x}^0$ is randomly chosen from the Pareto optimal set. Then, let $j = 0$, and go to step 2). Otherwise, go to the next step.

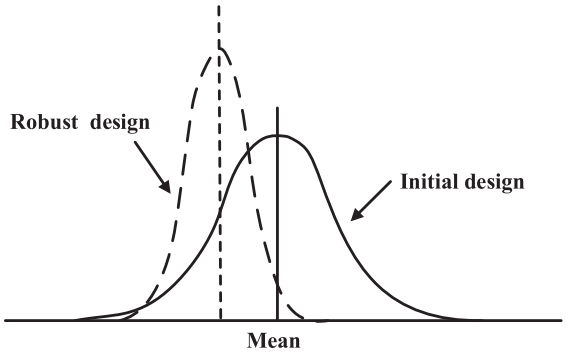

Fig. 5. Concept of the robust optimization design.

5) Decrease the temperature, and let $j = j+1$. If the iterative process is converged, the Pareto optimal set is output. Otherwise, go to step 2).

Fig. 6 illustrates a flowchart of the entire multi-objective robust optimization procedure under uncertainty for the SPT plant, and the detailed strategy procedure is given as follows.

1) **Establish the approximation model.** To improve computational efficiency, the response surface methodology is employed to construct the approximation function, which develops a relationship among the design parameters, uncertain parameters and SPT plant model output *LCOE*.
2) **Initialize the design parameters.** 12 design variables are selected for the SPT plant optimization, and their initial values are assigned randomly.
3) **Conduct the MC simulation.** To obtain the effect of 14 uncertain parameters on the SPT plant model output *LCOE*, the MC simulation is used to obtain the probability distribution of the *LCOE*. Then, the expected value and the standard deviation of the model output *LCOE* are obtained.
4) **Construct and solve the multi-objective robust optimization problem.** Considering the expected value and the standard deviation of *LCOE* as objective functions, the multi-objective robust optimization problem is formulated as described in Eq. (7). The SA algorithm is used to update the Pareto optimal set and the design parameters.
5) **Obtain the Pareto optimal set.** Repeat steps 3 to 4 until the convergence criterion is satisfied and the Pareto optimal set can be obtained.

5. Results and discussion

5.1. Model validation

The results of Collado and Guallar [36] are used here to validate the reliability of the deterministic model of the SPT plant system. The parameters of a 19.9 MW_e molten salt SPT plant with 2650 heliostats in Almeria are as follows: $\Delta\theta_1 = 0.136$ rad, $\Delta\theta_2 = 0.068$ rad, $\Delta\theta_3 = 0.034$ rad, $\Delta r_1 = 13.6$ m, $\Delta r_2 = 15.7$ m, $\Delta r_3 = 34.54$ m, $\Delta\gamma_1 = 15.7$ m, $\Delta\gamma_2 = 37.09$ m, $R = 4$ m, $THT = 140$ m, $H = 15$ h, $SM = 2.5$, $\alpha = 0.95$, $\varepsilon = 0.9$, $T_{amb} = 20$ °C, $A_{hel} = 115.5$ m^2. The two-tank thermal storage system is able to reach temperature up to 565 °C. The annual power block net efficiency is 0.3032 and related subsystem cost models are also given.

Table 3 shows comparison results of thermo-economic performance of a 19.9MW_e SPT plant. It exhibits that the simulation results of this paper agree well with the data in Ref. [36], and the relative error of *LCOE* is only 1.26 %.

5.2. Multi-objective robust optimization results under uncertainty

Fig. 7 depicts the Pareto frontier solutions for the multi-objective robust optimization of the SPT plant system under uncertainty. The expected value of *LCOE* represents an average energy cost, while the standard deviation of *LCOE* means the dispersion of energy cost and the sensitivity of energy cost to uncertainties. As shown in the figure, the improving one objective function degrades the other. Consequently, the SPT plant system design that is expected to be the least expensive can turn out to be a higher economic risk than others. In addition, the standard deviation of *LCOE* increases slightly when the expected value of *LCOE* decreases from 25.88 c/kWh_e to 23.09 c/kWh_e. A further decrement in the expected value of *LCOE* from 23.09 c/kWh_e to 21.92 c/kWh_e corresponds to a

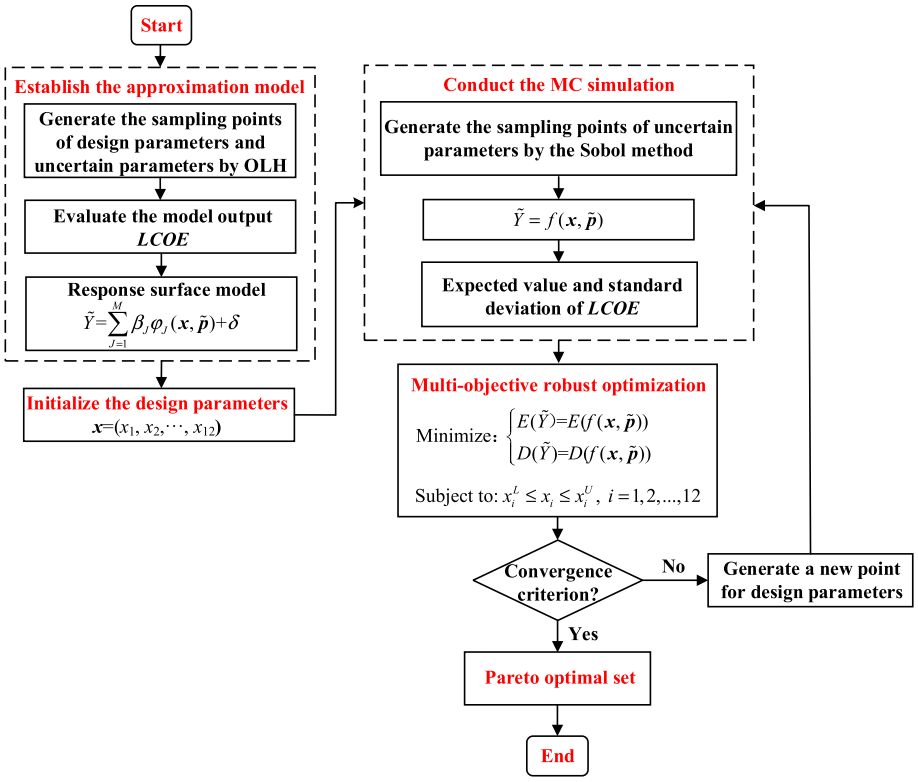

Fig. 6. Flowchart of the optimization procedure under uncertainty for the SPT plant.

Table 3
Comparisons of thermo-economic performance of a 19.9 MW_e SPT plant between the Ref [36] and this paper.

	Ref [36]	This paper	Relative difference
Annual heliostat field efficiency (%)	58.71 %	57.1 %	−2.74 %
Annual receiver efficiency (%)	89.16 %	90.14 %	1.1 %
Net annual electric output (GWh_e)	110.38 GWh_e	108.5 GWh_e	−1.7 %
LCOE (c/kWh_e)	23.72 c/kWh_e	24.02 c/kWh_e	1.26 %

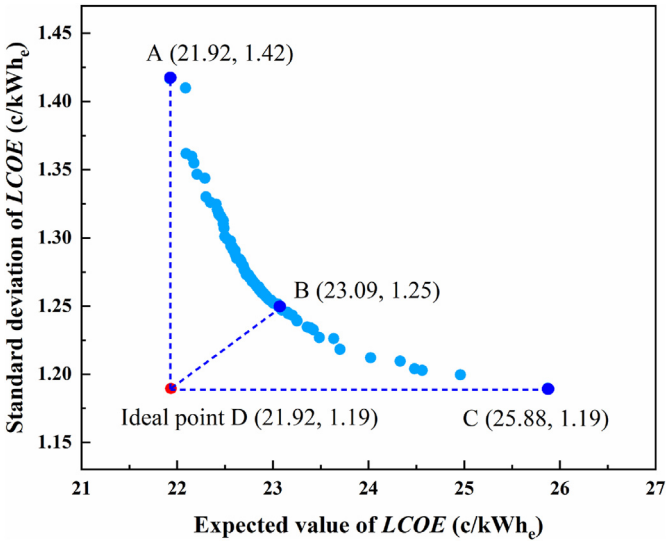

Fig. 7. Multi-objective optimization results of the SPT plant system under uncertainty.

drastic increase in the standard deviation of *LCOE*. Therefore, with a decreasing expected value of *LCOE*, the growth rate of the standard deviation of *LCOE* gradually increased.

Each point on the Pareto frontier represents an optimal solution of the SPT system design, and a decision-maker might select a different point based on the importance of each objective and engineering experience [47]. As shown in Fig. 7, design point A is the optimal solution when the decision-maker prefers to the minimum expected value of *LCOE*, while design point C represents the preference of the decision-maker that achieves the minimum standard deviation of *LCOE* and the lowest economic risk. The final multi-objective robust optimum is obtained with the aid of an ideal point D. The ideal point D meets the conditions of the minimum expected value of *LCOE* and the minimum standard deviation of *LCOE* simultaneously but is not one of the Pareto frontier solutions. Then, the design point B of the Pareto frontier is the closest to the ideal point D and chosen as the final multi-objective robust optimal point [48]. Consequently, the final optimal point B achieves the best trade-off between both optimization objectives. It should be noted that the final multi-objective robust optimum in this paper is decided by the preferences of the authors, and a different optimal

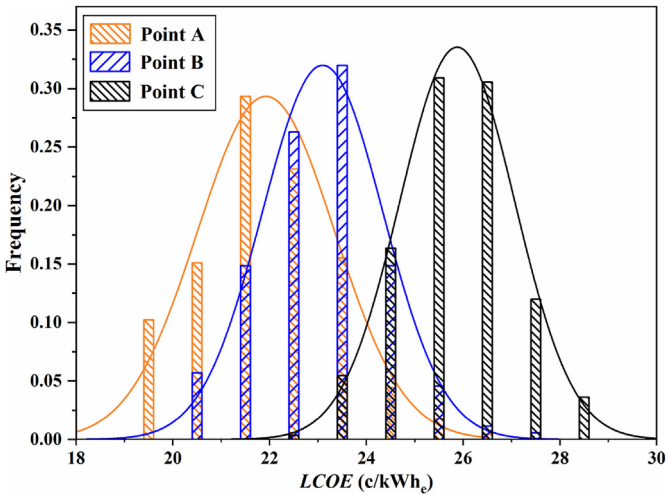

Fig. 8. Probability distributions of design points A, B and C based on uncertainty propagation.

point might be selected in another condition. To further demonstrate the robustness of the optimization result, probability distributions of design points A, B and C based on uncertainty propagation are shown in Fig. 8. Moreover, to guide the SPT system design under uncertainty, Table 4 presents the related design parameters at design points A, B and C.

5.3. Comparison results of the multi-objective robust and deterministic optimal design

The SA algorithm is adopted to optimize the deterministic model of the SPT system. Table 5 presents the related values of the design parameters under the deterministic optimal design.

Based on the uncertainty propagation of the SPT plant system, probability distributions of the deterministic and multi-objective robust optimum are compared in Fig. 9. It can be clearly seen that although the average model output *LCOE* of multi-objective robust solution is expected to be more expensive than that of deterministic solution, more stability exists in the multi-objective robust optimal design when faced with uncertainties, i.e. a lower risk of overestimating or underestimating *LCOE*.

To quantify the dispersion of the SPT plant system model output *LCOE* under uncertainty, Table 6 gives comparisons of the deterministic and multi-objective robust optimum according to the expectation and the variance of *LCOE*. The expected value of *LCOE* and the standard deviation of *LCOE* at deterministic optimal point are respectively 21.56 c/kWh$_e$ and 1.51 c/kWh$_e$, and those at multi-objective robust optimal point are respectively 23.09 c/kWh$_e$ and 1.25 c/kWh$_e$. Consequently, compared with the deterministic optimum, the multi-objective robust optimum reduces the standard deviation of *LCOE* by 17.22 % while only increasing the expected value of *LCOE* by 7.1 %. It further indicates that the multi-objective robust optimum exhibits less sensitivity to the uncertain system parameters and offers a better protection against economic risk at the cost of a slight increase in the expected value of *LCOE*. As a result, it is necessary to conduct multi-objective robust optimization of the SPT plant system by incorporating uncertainties.

Table 4
Related values of the design parameters at design points A, B and C.

	Point A	Point B	Point C
$\Delta\theta_1$ (rad)	$1.002l/r_1$	$1.001l/r_1$	$1.000l/r_1$
$\Delta\theta_2$ (rad)	$1.002l/r_2$	$1.000l/r_2$	$1.000l/r_2$
$\Delta\theta_3$ (rad)	$1.515l/r_3$	$1.514l/r_3$	$1.828l/r_3$
Δr_1 (m)	$0.867l$	$0.867l$	$0.868l$
Δr_2 (m)	$0.866l$	$0.867l$	$0.867l$
Δr_3 (m)	$2.235l$	$2.235l$	$2.203l$
$\Delta\gamma_1$ (m)	$0.948l$	$0.868l$	$0.963l$
$\Delta\gamma_2$ (m)	$2.399l$	$2.399l$	$2.400l$
R (m)	3.71	4.28	4.51
THT (m)	133	143	143
H (h)	11.88	9.59	7.03
SM (−)	2.69	2.7	2.7

Table 5
Related values of the design parameters under the deterministic optimal design.

$\Delta\theta_1$ (rad)	$1.001l/r_1$	$\Delta\gamma_1$ (m)	$0.869l$
$\Delta\theta_2$ (rad)	$1.000l/r_2$	$\Delta\gamma_2$ (m)	$2.398l$
$\Delta\theta_3$ (rad)	$1.419l/r_3$	R (m)	3.33
Δr_1 (m)	$0.866l$	*THT* (m)	138
Δr_2 (m)	$0.867l$	H (h)	11.97
Δr_3 (m)	$1.746l$	*SM* (−)	2.7

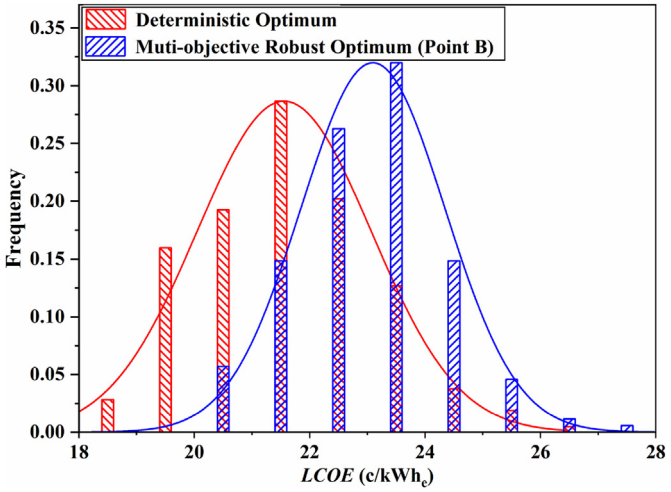

Fig. 9. Probability distributions of the deterministic and multi-objective robust optimum based on uncertainty propagation.

5.4. Sensitivity analysis of uncertainties

Based on the Pareto frontier solutions of the SPT plant system under uncertainty, the Sobol' global sensitivity method [49] is applied to evaluate the importance ranking of uncertainties and the interaction effects among uncertainties at design points A, B and C. According to the decomposition of the total variance of the complex nonlinear system model, the first-order sensitivity index (S_i) and the total sensitivity index (S_{Ti}) of each uncertain parameter are obtained. S_i represents the effect of individual uncertain parameter $\tilde{p}_i$ on *LCOE*, while S_{Ti} represents the impacts of $\tilde{p}_i$ and all its interactions. Therefore, (S_{Ti}−S_i) denotes the interaction effects of $\tilde{p}_i$

Table 6
Comparisons of the deterministic and multi-objective robust optimum based on uncertainty propagation.

	Deterministic optimum	Multi-objective robust optimum	Relative difference
expected value of *LCOE*	21.56 c/kWh$_e$	23.09 c/kWh$_e$	7.1 %
standard deviation of *LCOE*	1.51 c/kWh$_e$	1.25 c/kWh$_e$	−17.22 %

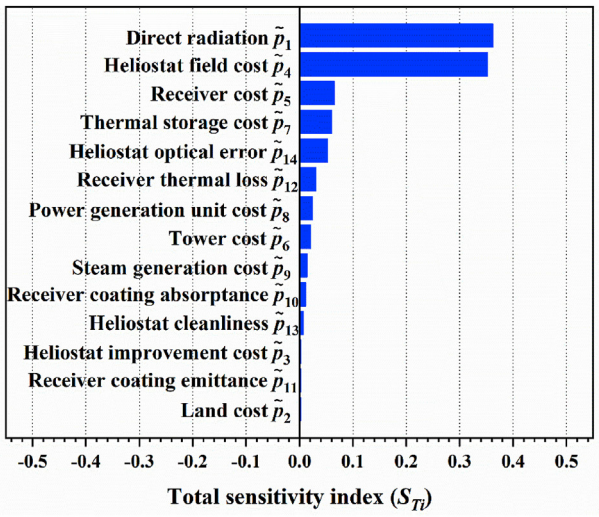

(a) Design point A

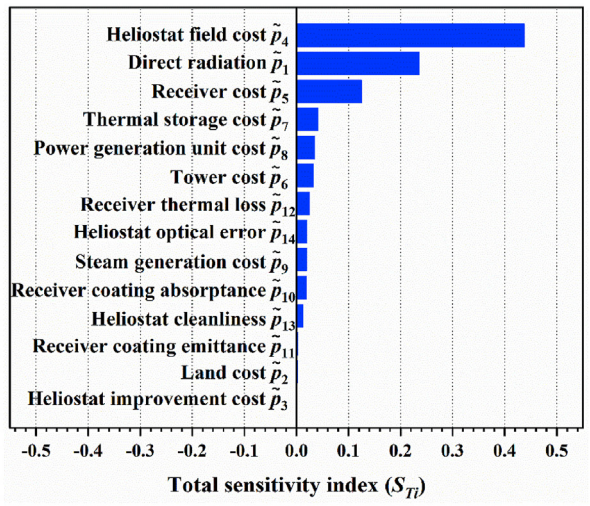

(b) Design point B

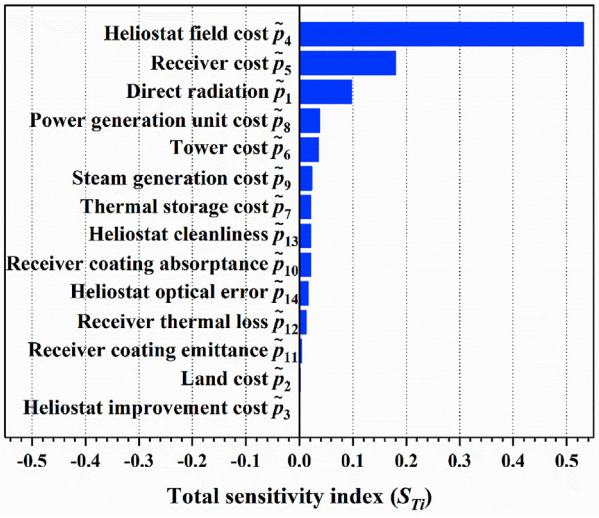

(c) Design point C

Fig. 10. Total sensitivity indices of uncertainties on *LCOE* at design points A, B and C.

Table 7
Global sensitivity analysis results at design point A.

	S_i	Rank	S_{Ti}	Rank	Contribution rate of S_{Ti}
$\tilde{p}_1$	0.3606	1	0.3613	1	36.1 %
$\tilde{p}_2$	0.0008	13	0.0015	14	0.1 %
$\tilde{p}_3$	0.0018	12	0.0022	12	0.2 %
$\tilde{p}_4$	0.3533	2	0.352	2	35.1 %
$\tilde{p}_5$	0.0678	3	0.0649	3	6.5 %
$\tilde{p}_6$	0.0209	8	0.0204	8	2.0 %
$\tilde{p}_7$	0.0592	4	0.0596	4	6.0 %
$\tilde{p}_8$	0.0225	7	0.0236	7	2.4 %
$\tilde{p}_9$	0.0135	9	0.014	9	1.4 %
$\tilde{p}_{10}$	0.0119	10	0.0116	10	1.2 %
$\tilde{p}_{11}$	0.0005	14	0.0019	13	0.2 %
$\tilde{p}_{12}$	0.0286	6	0.0298	6	3.0 %
$\tilde{p}_{13}$	0.0064	11	0.0069	11	0.7 %
$\tilde{p}_{14}$	0.0505	5	0.0519	5	5.1 %
Sum	0.9983		1.0016		100 %

Table 8
Global sensitivity analysis results at design point B.

	S_i	Rank	S_{Ti}	Rank	Contribution rate of S_{Ti}
$\tilde{p}_1$	0.2339	2	0.2349	2	23.5 %
$\tilde{p}_2$	0.0007	13	0.0015	13	0.1 %
$\tilde{p}_3$	0.0005	14	0.001	14	0.1 %
$\tilde{p}_4$	0.4391	1	0.4376	1	43.7 %
$\tilde{p}_5$	0.1284	3	0.1245	3	12.4 %
$\tilde{p}_6$	0.0327	6	0.0318	6	3.2 %
$\tilde{p}_7$	0.0406	4	0.041	4	4.1 %
$\tilde{p}_8$	0.0332	5	0.0347	5	3.5 %
$\tilde{p}_9$	0.0181	9	0.0188	8	1.9 %
$\tilde{p}_{10}$	0.019	8	0.0186	10	1.9 %
$\tilde{p}_{11}$	0.0008	12	0.0025	12	0.2 %
$\tilde{p}_{12}$	0.0227	7	0.024	7	2.3 %
$\tilde{p}_{13}$	0.0115	11	0.012	11	1.2 %
$\tilde{p}_{14}$	0.0171	10	0.0188	8	1.9 %
Sum	0.9983		1.0017		100 %

Table 9
Global sensitivity analysis results at design point C.

	S_i	Rank	S_{Ti}	Rank	Contribution rate of S_{Ti}
$\tilde{p}_1$	0.0961	3	0.0972	3	9.7 %
$\tilde{p}_2$	0.0009	13	0.0017	13	0.2 %
$\tilde{p}_3$	0	14	0.0007	14	0.1 %
$\tilde{p}_4$	0.5333	1	0.5314	1	53.1 %
$\tilde{p}_5$	0.1847	2	0.1795	2	17.9 %
$\tilde{p}_6$	0.0366	4	0.0353	5	3.5 %
$\tilde{p}_7$	0.0205	8	0.0208	7	2.1 %
$\tilde{p}_8$	0.0357	5	0.0374	4	3.7 %
$\tilde{p}_9$	0.022	6	0.0228	6	2.2 %
$\tilde{p}_{10}$	0.0213	7	0.0206	8	2.1 %
$\tilde{p}_{11}$	0.0018	12	0.0038	12	0.4 %
$\tilde{p}_{12}$	0.0111	11	0.0123	11	1.2 %
$\tilde{p}_{13}$	0.0202	9	0.0206	8	2.1 %
$\tilde{p}_{14}$	0.0151	10	0.0167	10	1.7 %
Sum	0.9993		1.0008		100 %

with other uncertainties [50].

The total sensitivity indices of uncertainties on *LCOE* at design points A, B and C are shown in Fig. 10. Tables 7–9 list the detailed global sensitivity analysis results at these three design points. At the three design points, it is possible to observe that the model output *LCOE* is most sensitive to the following uncertain parameters: direct radiation ($\tilde{p}_1$), heliostat field cost ($\tilde{p}_4$) and receiver cost ($\tilde{p}_5$). For instance, the contribution rates of S_{Ti} of these three uncertain parameters at design point A are 36.1 %, 35.1 % and 6.5 %, respectively, which account for 77.7 % of the total contribution. The

main reason might be that both $\tilde{p}_4$ and $\tilde{p}_5$ account for a large proportion of the total plant capital cost and $\tilde{p}_1$ has a significant influence on the annual electricity output of the SPT plant, which contribute to the *LCOE* as described in Eq. (3). Moreover, at design point A, S_{Ti} for $\tilde{p}_1$, $\tilde{p}_4$ and $\tilde{p}_5$ are 0.3613, 0.352 and 0.0649, respectively. S_{Ti} for $\tilde{p}_1$, $\tilde{p}_4$ and $\tilde{p}_5$ are 0.2349, 0.4376 and 0.1245, respectively, at design point B. At design point C, S_{Ti} for $\tilde{p}_1$, $\tilde{p}_4$ and $\tilde{p}_5$ are 0.0972, 0.5314 and 0.1795, respectively. Consequently, with an increasing expected value of *LCOE* (from point A to point C), the effects of $\tilde{p}_4$ and $\tilde{p}_5$ on *LCOE* are enhanced while the impacts of $\tilde{p}_1$ on *LCOE* decrease. This might occur because the total plant capital cost has a greater influence on *LCOE* than that of the annual electricity output with an increasing expected value of *LCOE*.

Additionally, land cost ($\tilde{p}_2$), heliostat improvement cost ($\tilde{p}_3$) and receiver coating emittance ($\tilde{p}_{11}$) are the most insensitive uncertainties at design points A, B and C. For instance, the contribution rates of S_{Ti} for $\tilde{p}_2$, $\tilde{p}_3$ and $\tilde{p}_{11}$ at design point A are 0.1 %, 0.2 % and 0.2 %, respectively, which are all less than 1 % of the total contribution. This is mainly because $\tilde{p}_{11}$ has little effect on the thermal efficiency of the receiver, and the investment for $\tilde{p}_2$ and $\tilde{p}_3$ accounts for a low proportion of the total plant capital cost. The importance rankings of other uncertain parameters vary with the design points. For example, the importance rankings of the heliostat optical error ($\tilde{p}_{14}$) are 5, 8 and 10 at design points A, B and C, respectively. The difference could be attributed to the lower impact of the annual electricity output on *LCOE* with an increase in the expected value of *LCOE*.

The sensitivity analysis results also show that almost no interaction effect exists in the uncertainties of the SPT plant system according to (S_{Ti}−S_i) and $\sum S_i$. On the one hand, in terms of design points A, B and C, the value of S_i is very close to the value of S_{Ti} for each of these uncertainties. For example, S_i and S_{Ti} for $\tilde{p}_1$ at design point A are 0.3606 and 0.3613, respectively, hence (S_{Ti}−S_i) is 0.0007. This negligible difference supports that there is almost no interaction between $\tilde{p}_1$ and other uncertainties. On the other hand, $\sum S_i$ at design points A, B and C are 0.9983, 0.9983 and 0.9993, respectively, which are very close to 1 and further suggest that the interaction effects among uncertainties are negligible.

6. Conclusions

In this paper, based on the MC simulation and SA algorithm, the multi-objective robust optimization of a molten salt SPT system under uncertainty is presented, which reveals the trade-off between the expected value and the standard deviation of *LCOE*. The main contributions of this work are summarized as follows.

(1) The Pareto frontier solutions are obtained for the multi-objective robust optimization of the SPT plant system under uncertainty, which indicate that a unique optimum does not exist and the final optimal solution is decided by the preference of the decision-maker. The one achieving the best trade-off between optimization objectives is selected with an expected value of *LCOE* of 23.09 c/kWh$_e$ and a standard deviation of *LCOE* of 1.25 c/kWh$_e$.

(2) Compared with the deterministic optimal design, the multi-objective robust optimum reduces the standard deviation of *LCOE* by 17.22 % while only increasing the expected value of *LCOE* by 7.1 %. It indicates that the multi-objective robust optimum is less sensitive to the uncertainties and offers a better protection against economic risk.

(3) The global sensitivity analysis results of uncertainties demonstrate that direct radiation, heliostat field cost and receiver cost have the greatest effects on the model output *LCOE* at different design points, while the impacts of land cost, heliostat improvement cost and receiver coating emittance are the lowest. The interaction effects of all the uncertain parameters are almost negligible.

Credit author statement

Yan Luo: Conceptualization, Methodology, Software, Resources, Writing-Original Draft.

Zhiyuan Wang: Software, Investigation, Writing-Review & Editing.

Jiamin Zhu: Software, Writing-Review & Editing.

Tao Lu: Formal Analysis, Data Curation.

Gang Xiao: Validation, Investigation, Data Curation.

Fengming Chu: Writing: Review & Editing, Supervision.

Ruixing Wang: Methodology, Supervision.

Declaration of competing interest

The authors declare that they have no known competing financial interests or personal relationships that could have appeared to influence the work reported in this paper.

Acknowledgment

The financial supports for this research project from the National Natural Science Foundation of China (No. 51806009) and the State Key Laboratory of Clean Energy Utilization (No. ZJUCEU2020019) is gratefully acknowledged.

References

[1] Behar O, Khellaf A, Mohammedi K. A review of studies on central receiver solar thermal power plants. Renew Sustain Energy Rev 2013;23:12−39.
[2] Agency IE. Technology roadmap: solar thermal electricity. Paris, France: IEA; 2014.
[3] Yang HL, Li J, Huang YH, Kwan TH, Cao JY, Pei G. Feasibility research on a hybrid solar tower system using steam and molten salt as heat transfer fluid. Energy 2020;205:118094.
[4] Spelling J, Favrat D, Martin A, Augsburger G. Thermoeconomic optimization of a combined-cycle solar tower power plant. Energy 2012;41(1):113−20.
[5] Ramos A, Ramos F. Strategies in tower solar power plant optimization. Sol Energy 2012;86(9):2536−48.
[6] Luo Y, Lu T, Du XZ. Novel optimization design strategy for solar power tower plants. Energy Convers Manag 2018;177:682−92.
[7] Wang K, He YL. Thermodynamic analysis and optimization of a molten salt solar power tower integrated with a recompression supercritical CO2 Brayton cycle based on integrated modeling. Energy Convers Manag 2017;135:336−50.
[8] Carrizosa E, Dominguez-Bravo C, Fernandez-Cara E, Quero M. Optimization of multiple receivers solar power tower systems. Energy 2015;90:2085−93.
[9] Khosravi A, Malekan M, Pabon JJG, Zhao X, Assad MEH. Design parameter modelling of solar power tower system using adaptive neuro-fuzzy inference system optimized with a combination of genetic algorithm and teaching learning-based optimization algorithm. J Clean Prod 2020;244:118904.
[10] Muller SC, Remund J. Solar radiation and uncertainty information of meteonorm 7. In: Proceedings of 26th European photovoltaic solar energy conference and exhibition; 2011. p. 4388−90.
[11] Remund J. Quality of meteonorm version 6.0. Europe 2008;6(1):389.
[12] Ho CK, Kolb GJ. Incorporating uncertainty into probabilistic performance models of concentrating solar power plants. J Sol Energ-T ASME 2010;132(3):533−42.
[13] Ho CK, Khalsa SS, Kolb GJ. Methods for probabilistic modeling of concentrating solar power plants. Sol Energy 2011;85(4):669−75.
[14] Ho CK, Mehos M, Turchi C, Wagner M. Probabilistic analysis of power tower systems to achieve SunShot goals. Energy Procedia 2014;49:1410−9.
[15] Boubault A, Ho CK, Hall A, Lambert TN, Ambrosini A. Durability of solar absorber coatings and their cost-effectiveness. Sol Energy Mater Sol Cell 2017;166:176−84.
[16] Meybodi MA, Beath A. Impact of cost uncertainties and solar data variations on the economics of central receiver solar power plants: an Australian case study. Renew Energy 2016;93:510−24.
[17] Zaversky F, Garci'a-Barberena J, Sa'nchez M, Astrain D. Probabilistic modeling of a parabolic trough collector power plant - an uncertainty and sensitivity

analysis. Sol Energy 2012;86(7):2128–39.
[18] Silva R, Perez MS, Berenguel M, Valenzuela L, Zarza E. Uncertainty and global sensitivity analysis in the design of parabolic-trough direct steam generation plants for process heat applications. Appl Energy 2014;121:233–44.
[19] Nojavan S, Pashaei-Didani H, Saberi K, Zare K. Risk assessment in a central concentrating solar power plant. Sol Energy 2019;180:293–300.
[20] Beyer HG, Sendhoff B. Robust optimization-a comprehensive survey. Comput Methods Appl Math 2007;196(33–34):3190–218.
[21] Ben-Tal A, Nemirovski A. Robust optimization–methodology and applications. Math Program 2002;92(3):453–80.
[22] Wang M, Yu H, Jing R, Liu H, Chen P, Li C. Combined multi-objective optimization and robustness analysis framework for building integrated energy system under uncertainty. Energy Convers Manag 2020;208:1–15.
[23] Akbari K, Nasiri MM, Jolai F, Ghaderi SF. Optimal investment and unit sizing of distributed energy systems under uncertainty: a robust optimization approach. Energy Build 2014;85:275–86.
[24] Reich M, Adam M, Gottschald J. Robust optimization of district heating networks structure and dimension combining metamodels and multi-objective optimization. In: Proceedings of the ECOS; 2018 [Guimaraes, Portugal].
[25] Sy CL, Aviso KB, Ubando AT, Tan RR. Target-oriented robust optimization of polygeneration systems under uncertainty. Energy 2016;116:1334–47.
[26] Serafino A, Obert B, Vergé L, Cinnella P. Robust optimization of an organic Rankine cycle for geothermal application. Renew Energy 2020;161:1120–9.
[27] Gang W, Augenbroe G, Wang S, Fan C, Xiao F. An uncertainty-based design optimization method for district cooling systems. Energy 2016;102:516–27.
[28] Niu J, Tian Z, Lu Y, Zhao HF, Lan B. A robust optimization model for designing the building cooling source under cooling load uncertainty. Appl Energy 2019;241:390–403.
[29] Tian W. A review of sensitivity analysis methods in building energy analysis. Renew Sustain Energy Rev 2013;20:411–9.
[30] Wagner MJ, Hamilton WT, Newman A, Dent J, Diep C, Braun R. Optimizing dispatch for a concentrated solar power tower. Sol Energy 2018;174:1198–211.
[31] Eck M, Feldhoff JF, Kretschmann D, Wittmann M, Schenk H. Considering uncertainties in research by probabilistic modeling. In: ASME 2012 6th international conference on energy sustainability, es2012-91055; 2012. p. 263–71 [San Diego, USA].
[32] Atif M, Alsulaiman FA. Optimization of heliostat field layout in solar central receiver systems on annual basis using differential evolution algorithm. Energy Convers Manag 2015;95:1–9.
[33] Singer C, Buck R, Pitz-Paal R, Müller-Steinhagen H. Assessment of solar power tower driven ultrasupercritical steam cycles applying tubular central receivers with varied heat transfer media. J Sol Energ-T ASME 2010;132(4):41010.
[34] Siebers DL, Kraabel JS. Estimating convective energy losses from solar central receivers. Livermore, USA: Sandia National Laboratories; 1984.
[35] Ye T. Thermal power stations. China Electric Power Press; 2009 [in Chinese)].
[36] Collado FJ, Guallar J. Two-stages optimised design of the collector field of solar power tower plants. Sol Energy 2016;135:884–96.
[37] Montes MJ, Abanades A, Martinez-Val JM, Valdes M. Solar multiple optimization for a solar-only thermal power plant, using oil as heat transfer fluid in the parabolic trough collectors. Sol Energy 2009;83(12):2165–76.
[38] Solar advisor model (SAM). Version 2015.6.30. National Renewable Energy Laboratory.
[39] Noone CJ, Torrilhon M, Mitsos A. Heliostat field optimization: a new computationally efficient model and biomimetic layout. Sol Energy 2012;86(2):792–803.
[40] Robert C, Casella G. Monte Carlo statistical methods. Springer; 2013.
[41] Saltelli A, Ratto M, Andres T, Campolongo F, Tarantola S. Global sensitivity analysis: the primer. England: John Wiley & Sons; 2008.
[42] Makela M. Experimental design and response surface methodology in energy applications: a tutorial review. Energy Convers Manag 2017;151:630–40.
[43] Devanathan S, Koch PN. Comparison of meta-modeling approaches for optimization. In: ASME international mechanical engineering congress and exposition, IMECE2011-65541; 2011. p. 827–35 [Colorado, USA].
[44] Suppapitnarm A, Seffen KA, Parks GT, Clarkson PJ. A simulated annealing algorithm for multiobjective optimization. Eng Optim 2000;33(1):59–85.
[45] Kirkpatrick S, Gelatt CD, Vecchi MP. Optimization by simulated annealing. Science 1983;220(4598):671–80.
[46] Alcantar V, Aceves SM, Ledesma E, Ledesma S, Aguilera E. Optimization of type 4 composite pressure vessels using genetic algorithms and simulated annealing. Int J Hydrogen Energy 2017;42(24):15770–81.
[47] Sayyaadi H, Amlashi EH, Amidpour M. Multi-objective optimization of a vertical ground source heat pump using evolutionary algorithm. Energy Convers Manag 2009;50(8):2035–46.
[48] Wang M, Wang JF, Zhao P, Dai YP. Multi-objective optimization of a combined cooling, heating and power system driven by solar energy. Energy Convers Manag 2015;89:289–97.
[49] Sobol IM. Sensitivity estimates for nonlinear mathematical models. Math Model Civ Eng 1993;1:407–14.
[50] Zhan Y, Zhang M. Application of a combined sensitivity analysis approach on a pesticide environmental risk indicator. Environ Model Software 2013;49:129–40.